AIAA JOURNAL
Vol. 42, No. 4, April 2004

Prediction of Sound Propagation in Ducted Potential Flows Using Green's Function Discretization

Damiano Casalino*
Fluorem, 69134 Ecully Cedex, France
and
Michel Roger† and Marc C. Jacob‡
Ecole Centrale de Lyon, 69134 Ecully Cedex, France

The sound propagation in ducted mean potential flows is computed by using a Green's function discretization (GFD) technique. Linear combinations of the free-space Green's functions of the locally uniform convected Helmholtz problem are analytically differentiated to build shape functions for the derivatives of the acoustic potential. These are used to discretize both the field governing equation and the boundary conditions. The GFD approach is validated by computing the sound propagation in annular ducts with hard/soft walls and uniform flow. Acoustic modes of increasing wave number are computed without changing the computational mesh. A good level of accuracy is ensured up to three points per wavelength. As a first step toward relevant applications, the propagation in nonconstant annular ducts, with/without wall treatment and with/without flow, is computed. The numerical solutions compare favorably with the well-known analytical multiscale solutions.

Nomenclature

$\mathcal{A}, \mathcal{B}_i, \mathcal{C}$	=	coefficients of wave equation (5)
a^i_m, b^i	=	coefficients of a discretized equation at node i
c	=	sound speed
$F_m, \mathcal{F}_m$	=	mth discretization coefficient of ϕ
G	=	convected Green's function
$\mathcal{G}$	=	soft-wall annular duct mode
i	=	imaginary unit
k	=	acoustic wave number
$\boldsymbol{M}$	=	dimensionless mean flow velocity
M^i	=	number of nodes in the ith stencil
N	=	number of fictitious sources (or duct modes)
$\hat{\boldsymbol{n}}$	=	normal unit vector
P, Θ, Φ	=	mean-flow pressure, density, and potential
p, ρ, ϕ	=	acoustic pressure, density, and potential
q, σ	=	circumferential and radial mode orders
r, θ, z	=	cylindrical coordinates
$\mathcal{Z}$	=	wall impedance
β	=	Prandtl–Glauert factor
γ	=	specific heats ratio
γ_n	=	intensity of the nth fictitious source (or mode)

Subscripts

m	=	mth node influence coefficient
n	=	nth source (or duct mode)
X, Y, Z	=	shape functions of space derivatives
∞	=	undisturbed flow quantity

Superscripts

I	=	pseudoinverse matrix element
i	=	evaluation at the node i
$+$	=	right-moving propagation
$-$	=	left-moving propagation

Received 19 March 2003; presented as Paper 2003-3246 at the AIAA/CEAS 9th Aeroacoustics Conference, Hilton Head, SC, 13 May 2003; revision received 13 November 2003; accepted for publication 18 December 2003.

*Aerospace Engineer.
†Professor, Laboratoire de Mécanique des Fluides et d'Acoustique.
‡Assistant Professor, Laboratoire de Mécanique des Fluides et d'Acoustique; currently Assistant Professor, Université C. Bernard, 69100 Villeurbanne, France.

Introduction

RECENT trends to increase the bypass ratio of civil transport turbofans are expected to further increase the fan contribution to the overall noise. Therefore, inlet geometry optimization, acoustic lining, and active control have become a serious concern of aeroengine manufacturers.

The sound transmission in a ducted mean flow is a complex problem. Some relevant effects of the mean flow on the sound propagation can be mentioned:

1) A viscous boundary layer modifies the acoustic impedance of a solid surface. For a boundary-layer thickness much smaller than the acoustic wavelength, an expression of the wall impedance was obtained by Tester.[1]

2) Myers[2] showed that, for a mean potential flow with superimposed acoustic disturbances, the acoustic boundary condition at an impedance wall must account for the flow velocity and its space derivatives.

3) Due to the flow nonuniformity, the sound propagation in a varying-area duct is described by a wave equation with nonconstant coefficients. This reduces the possibility of obtaining solutions in terms of a modal expansion.

4) In turbomachinery configurations, the flow has a nonnegligible swirling motion. Golubev and Atassi[3] showed that an irrotational swirling flow affects the duct modal behavior: the Doppler frequency shift enables evanescent spinning modes (especially those opposite to the swirl) to propagate both upstream and downstream. Moreover, as further discussed by Golubev and Atassi,[4] the presence of a mean rotational swirling flow causes the acoustic and vorticity modes to be coupled.

Rienstra's[5] analysis revealed that the modal sound transmission in a nonswirling mean potential flow in a duct with slowly varying properties (cross section, flow, wall impedance) has an approximated multiscale solution. This was tested by Rienstra and Eversman[6] against a finite element solution of the same potential flow problem for configurations that are representative of high-bypass turbofan engines. A good agreement was obtained also for high wave numbers and low circumferential mode orders when scattering into higher radial modes can occur easily.

For hard-wall circular ducts, Rienstra's analysis was extended by Cooper and Peake[7] to account for a rotational swirl in the mean

flow. The resulting multiscale solution is more complicated than the irrotational one, because the problem is not self-adjoint.

The multiscale approach, as developed by Rienstra, Cooper, and Peake, is an essential tool for the design and optimization of a quiet turbofan lined inlet. However, numerical predictions of sound transmission in ducted flows must still be carried out for generic configurations involving nonslowly varying parameters, generic flows, and nonaxisymmetric geometries. Again, the multiscale solution can be used for a preliminary validation of the numerical methods employed.

In this paper we investigate the feasibility of a low-cost Green's function discretization (GFD) prediction of a duct acoustic field by solving the acoustic potential equation linearized around a potential mean flow. The GFD scheme is the same used by Di Francescantonio and Casalino[8] for sound propagation in external nonuniform flows. It consists of using elementary solutions (Green's functions) of the locally uniform convected Helmholtz problem as local shape functions tailored to the wave propagation problem. Hard- and soft-wall annular ducts are considered to assess the GFD code Grefundia.[9] Convergence tests are carried out by computing hard- and soft-wall duct modes of increasing wave number without changing the computational mesh. Good results are obtained for up to three grid points per acoustic wavelength.

As a primary step toward applications of practical interest, the sound transmission through an annular duct of varying cross section is computed for four configurations: 1) hard-wall duct without flow, 2) soft-wall duct without flow, 3) hard-wall duct with flow, and 4) soft-wall duct with flow. Numerical results are checked against the analytical multiscale solution.[5]

Physical Model

Consider a compressible inviscid perfect isentropic irrotational gas mean flow with superimposed linear harmonic acoustic disturbances of angular frequency ω. The flow density $\tilde{\rho}$, pressure $\tilde{p}$, velocity $\tilde{\boldsymbol{v}}$, and velocity potential $\tilde{\phi}$ can be split into mean (stationary) parts and acoustic perturbations; that is,

$$\tilde{\rho} = \Theta + \rho \mathrm{e}^{-\mathrm{i}\omega t} \tag{1}$$

$$\tilde{p} = P + p\mathrm{e}^{-\mathrm{i}\omega t} \tag{2}$$

$$\tilde{\boldsymbol{v}} = c_\infty \boldsymbol{M} + \boldsymbol{\nabla}\phi \mathrm{e}^{-\mathrm{i}\omega t}, \qquad \text{with} \qquad \boldsymbol{\nabla}\Phi = c_\infty \boldsymbol{M} \tag{3}$$

where $\boldsymbol{M} = \boldsymbol{U}/c_\infty$ is the local dimensionless mean flow velocity and $c_\infty = (\gamma p_\infty/\rho_\infty)^{1/2}$ is the sound speed in the uniform (undisturbed) mean flow, where pressure, density, and Mach number are p_∞, ρ_∞, and $\boldsymbol{M}_\infty$, respectively.

Linearization of the flow governing equation yields a relationship between the acoustic pressure and the acoustic potential, that is,

$$p = \rho_\infty c_\infty (1-\mathcal{A})^{1/(\gamma-1)} \left[\mathrm{i}k\phi - M_i \frac{\partial \phi}{\partial x_i} \right] \tag{4}$$

and an equation for the acoustic potential (see, e.g., Refs. 9 and 10), that is,

$$(1-\mathcal{A})\frac{\partial^2\phi}{\partial x_i^2} - M_i M_j \frac{\partial^2 \phi}{\partial x_i \partial x_j} + (\mathrm{i}\,2kM_i - \mathcal{B}_i - M_i\mathcal{C})\frac{\partial \phi}{\partial x_i} + k(k+\mathrm{i}\mathcal{C})\phi = 0 \tag{5}$$

where $k = \omega/c_\infty$ is the acoustic wave number and the coefficients $\mathcal{A} = (\gamma-1)(M^2 - M_\infty^2)/2$, $\mathcal{B}_i = 2\,M_j \partial M_j/\partial x_i$, and $\mathcal{C} = (\gamma-1)\,\partial M_j/x_j$ account for the local nonuniformity of the mean flow, which has local thermodynamic properties

$$P = p_\infty (1-\mathcal{A})^{\gamma/(\gamma-1)} \tag{6}$$

$$\Theta = \rho_\infty (1-\mathcal{A})^{1/(\gamma-1)} \tag{7}$$

In Eqs. (4) and (5), use of Einstein's convention of index summation has been made.

If the mean flow is uniform (as in a duct of constant cross section), Eqs. (4) and (5) take the form

$$p = \rho_\infty c_\infty \left(\mathrm{i}k\phi - M_i \frac{\partial \phi}{\partial x_i} \right) \tag{8}$$

$$\frac{\partial^2\phi}{\partial x_i^2} - M_i M_j \frac{\partial^2 \phi}{\partial x_i \partial x_j} + i2kM_i \frac{\partial \phi}{\partial x_i} + k^2\phi = 0 \tag{9}$$

Throughout, Eq. (9) is referred to as the convected Helmholtz equation.

In this paper we are concerned with the acoustic transmission through ducts with soft walls. The impedance condition

$$k\nabla\phi\cdot\hat{\boldsymbol{n}} + [k + i\boldsymbol{M}\cdot\nabla - i\hat{\boldsymbol{n}}\cdot(\hat{\boldsymbol{n}}\cdot\nabla\boldsymbol{M})](p/\mathcal{Z}) = 0 \tag{10}$$

is therefore imposed on the duct surfaces. This condition was obtained by Myers[2] for a potential flow bounded by a smoothly curved surface of acoustic impedance $\mathcal{Z}$ and normal unit vector $\hat{\boldsymbol{n}}$ pointing into the wall.

Discretization Scheme

The GFD scheme developed by Di Francescantonio and Casalino[8] is based on the interpolation formula proposed by Caruthers et al.[11] for the Helmholtz equation $(\nabla^2 + k^2)\phi = 0$. The formula was first adapted to a convected wave propagation and was then used to obtain a discretization scheme for Eq. (5).

Consider a generic domain $\mathcal{D}_m$ in which the acoustic potential ϕ satisfies the convected Helmholtz equation, and suppose that the values $\phi_m = \phi(\boldsymbol{x}_m)$ are given in a certain number M of points $\boldsymbol{x}_m$ inside $\mathcal{D}_m$. We are interested in modeling the potential field $\phi(\boldsymbol{x})$ in the region $\mathcal{D}_m$ by using the given values ϕ_m.

Following the work of Caruthers et al.,[11] we can assume that the potential field is produced by an arbitrary distribution of N elementary sources, each having intensity γ_n and position $\boldsymbol{x}_n$. Therefore, let us write

$$\phi(\boldsymbol{x}) = \sum_{n=1}^{N} \gamma_n G(\boldsymbol{x}, \boldsymbol{x}_n; \boldsymbol{M}) \tag{11}$$

where $G(\boldsymbol{x}, \boldsymbol{x}_n; \boldsymbol{M})$ is the Green's function of Eq. (9). Setting $r = |\boldsymbol{x} - \boldsymbol{x}_n|$, $M_r = \boldsymbol{M}\cdot(\boldsymbol{x}-\boldsymbol{x}_n)/r$, and $\beta = \sqrt{(1-M^2)}$, it reads

$$G(\boldsymbol{x}, \boldsymbol{x}_n; \boldsymbol{M}) = \frac{\exp\left[(ikr/\beta^2)\left(-M_r + \sqrt{M_r^2 + \beta^2}\right)\right]}{r\sqrt{M_r^2 + \beta^2}} \tag{12}$$

where the constant has been absorbed by γ_n. Requiring the satisfaction of Eq. (11) at each point $\boldsymbol{x}_m$ yields a set of M compatibility conditions:

$$\phi_m = \sum_{n=1}^{N} \gamma_n G_{mn}, \qquad m = 1, M \tag{13}$$

where $G_{mn} = G(\boldsymbol{x}_m, \boldsymbol{x}_n; \boldsymbol{M})$. By fixing the source positions $\boldsymbol{x}_n$, for instance, on the surface of a sphere centered in $\boldsymbol{x}$, Eq. (13) yields a linear system relating the N unknown γ_n to the M values ϕ_m. Although a unique solution can exist only if $N = M$, Caruthers et al.[11] proposed to use $N > M$ to improve the quality of the reconstruction. Indeed, among the infinite solutions γ_n of system (13), we can choose the one that ensures the values ϕ_m with a minimum cancellation inside $\mathcal{D}_m$. This intensity distribution is reasonably expected to satisfy a condition of minimum variation in the norm L^2 (minimum $\sum_n \gamma_n^2$), a condition that can be indirectly imposed by computing the pseudoinverse matrix G^I_{nm} of G_{mn}. The source intensities are thus given by

$$\gamma_n = \sum_{m=1}^{M} G^I_{nm}\phi_m, \qquad n = 1, N \tag{14}$$

Substituting Eq. (14) into Eq. (11) and commuting the sum operators yields

$$\phi(\boldsymbol{x}) = \sum_{m=1}^{M} F_m(\boldsymbol{x})\phi_m \tag{15}$$

where the functions

$$F_m(\boldsymbol{x}) = \sum_{n=1}^{N} G^I_{nm} G(\boldsymbol{x}, \boldsymbol{x}_n; \boldsymbol{M}), \qquad m = 1, M \tag{16}$$

play the role of shape functions tailored to the acoustic problem. Equation (15) is the interpolation formula proposed by Caruthers et al.[11] with a minor modification to account for the convective effects.

Consider a discretized domain and let $\boldsymbol{x}^i_m$ denote one of the M^i nodes constituting the stencil of the node $\boldsymbol{x}^i$. Suppose that the node i itself is considered to be within the M^i nodes. Two strategies are now presented, which allow formulation of a discretization scheme based on Eq. (15). The first can be derived from the work of Caruthers et al.[11]; the second was proposed by Di Francescantonio and Casalino.[8]

Caruthers et al. Scheme

Interpolation formula (15) can be regarded as a compatibility condition between the acoustic potential at the M^i nodes of the stencil i. Because the verification of Eq. (9) is ensured by the fact that shape functions (16) are combinations of elementary solutions of the same governing equation, a solution of Eq. (9) can be obtained by only requiring the verification of some boundary conditions. This is the approach used by Caruthers et al.[11] that leads to the following discretization scheme:

$$\sum_{m=1}^{M^i} a^i_m \phi^i_m = 0, \qquad \text{with} \qquad a^i_m = \begin{cases} 1 & \text{if } \boldsymbol{x}^i_m \equiv \boldsymbol{x}^i \\ -F^i_m & \text{otherwise} \end{cases} \tag{17}$$

where the influence coefficients of $F^i_m = F_m(\boldsymbol{x})^i$ must be computed by excluding the node i from its stencil.

Numerical results[11,12] show that this GFD scheme is able to reconstruct an acoustic field with only two to three points per wave. However, it can be applied only in cases for which the Green's function of the governing equation is known or when it can be computed in an approximate form.[13]

Di Francescantonio and Casalino Scheme

A more general GFD approach consists of effectively discretizing Eq. (9) by means of shape functions for the derivatives of $\phi(\boldsymbol{x})$, obtained by differentiating shape functions (16). For example, the first-order x derivative reads

$$\phi_x(\boldsymbol{x}) = \sum_{m=1}^{M} F_{mX}(\boldsymbol{x})\phi_m \tag{18}$$

with

$$F_{mX}(\boldsymbol{x}) = \sum_{n=1}^{N} G^I_{nm} G_x(\boldsymbol{x}, \boldsymbol{x}_n; \boldsymbol{M}), \qquad m = 1, M \tag{19}$$

Therefore, by using a collocation technique to discretize Eq. (9), we obtain a linear system

$$\sum_{m=1}^{M} a^i_m \phi^i_m = 0$$

with coefficients

$$\begin{aligned} a^i_m = {} & \left(1 - M_x^2\right) F^i_{mXX} + \left(1 - M_y^2\right) F^i_{mYY} + \left(1 - M_z^2\right) F^i_{mZZ} \\ & - 2M_x M_y F^i_{mXY} - 2M_x M_z F^i_{mXZ} - 2M_y M_z F^i_{mYZ} \\ & + i2k\left(M_x F^i_{mX} + M_y F^i_{mY} + M_z F^i_{mZ}\right) + k^2 F^i_m \end{aligned} \tag{20}$$

The node i can be considered to be within the M^i nodes of its stencil. In this case the influence coefficients of ϕ^i verify the following property:

$$F^i_m = \begin{cases} 1 & \text{if } \boldsymbol{x}^i_m \equiv \boldsymbol{x}^i \\ 0 & \text{otherwise} \end{cases} \tag{21}$$

As pointed out in Ref. 8 all the coefficients a^i_m in Eq. (20) are identically null, as obtained by differentiating elementary solutions of the governing equation. Some corrective action is therefore necessary for the method to make sense. The strategy adopted in this paper is to distribute the fictitious sources over two spheres, the first having a smaller radius and containing a larger number of sources and the second having a greater radius and containing only a few sources. Furthermore, the second sphere is indeed a four-dimensional hypersphere, and a four-dimensional norm is used to evaluate the term $r = |\boldsymbol{x}_n - \boldsymbol{x}|$ in the Green's function. This prevents the shape functions from being exact solutions of the governing equation without spoiling their suitability to describe a wave field. Some details concerning this GFD approach and the hypersphere are reported in Appendices A and B.

Boundary Conditions

Boundary conditions given as analytical expressions involving the potential and its derivatives can be discretized by using the same shape functions used for the governing equation, according to Di Francescantonio and Casalino's GFD approach. The node i can thus be considered to be within the M^i nodes of its stencil, and three-dimensional distributions of fictitious sources can be used, because the shape functions do not verify the boundary conditions. This approach is used in this paper to discretize Myers's impedance condition (10).

A different approach, which is closer to the Caruthers et al. GFD method, is used to formulate inlet/exhaust conditions for the duct terminations. Suppose that the duct considered is a portion of an infinite soft-wall duct inside which the acoustic field has the general modal form (see Appendix C)

$$\phi(\boldsymbol{x}) = \sum_{n=1}^{N} \gamma_n \mathcal{G}_n(\boldsymbol{x})$$

with

$$\mathcal{G}_n(\boldsymbol{x}) = \Phi_n(z, r) \exp\left(iq\theta + i \int^z \mu_n(\xi)\, \mathrm{d}\xi \right) \tag{22}$$

where $n = n(q, \sigma)$ denotes a cumulative mode order index, and q and σ are the circumferential and radial mode orders, respectively. Suppose that the total number of radial and circumferential modes is such that $N > M$, with M denoting a certain number of given values ϕ_m at points in the neighborhood of $\boldsymbol{x}$, where the acoustic field has modal structure (22). Therefore, we can write a set of M compatibility conditions:

$$\phi_m = \sum_{n=1}^{N} \gamma_n \mathcal{G}_n(\boldsymbol{x}_m) = \sum_{n=1}^{N} \gamma_n \mathcal{G}_{mn}, \qquad m = 1, M \tag{23}$$

By least-squares inversion we obtain

$$\gamma_n = \sum_{m=1}^{M} \mathcal{G}^I_{nm} \phi_m, \qquad n = 1, N \tag{24}$$

Finally, substitution in Eq. (22) yields the interpolation formula

$$\phi(\boldsymbol{x}) = \sum_{m=1}^{M} \mathcal{F}_m(\boldsymbol{x})\phi_m \tag{25}$$

where

$$\mathcal{F}_m(\boldsymbol{x}) = \sum_{n=1}^{N} \mathcal{G}^I_{nm} \mathcal{G}_n(\boldsymbol{x}), \qquad m = 1, M \tag{26}$$

are shape functions that ensure the required modal structure of the acoustic field in the neighborhood of $\boldsymbol{x}$. Interpolation formula (25) is now used to obtain inlet/exhaust nonreflecting conditions.

Nonreflecting Exhaust Duct Condition

This condition consists of using formula (25) as a compatibility condition between the potential at the node i and the potential at the other nodes of the stencil. Therefore, for example, a right-outgoing propagation without ingoing reflections can be discretized as

$$\sum_{m=1}^{M^i} a_m^i \phi_m^i = 0$$

with

$$a_m^i = \begin{cases} 1 & \text{if} \quad \boldsymbol{x}_m^i \equiv \boldsymbol{x}^i \\ -\mathcal{F}_m^{+i} & \text{otherwise} \end{cases} \tag{27}$$

where

$$\mathcal{F}_m^{+i} = \sum_{n=1}^{N} \mathcal{G}_{nm}^{+I} \mathcal{G}_n^+(\boldsymbol{x}^i) \tag{28}$$

$$\mathcal{G}_n^+(\boldsymbol{x}^i) = \Phi_n(z^i, r^i) \exp\left(iq\theta^i + i \int^{z^i} \mu_n(\xi)\, \mathrm{d}\xi \right) \tag{29}$$

Nonreflecting Inlet Duct Condition

This condition consists of imposing an incident wave on the inlet section without blocking the outgoing propagation of a possible backscattered wave. Consider, for example, a right-going incident wave ϕ_{inc}. A nonreflecting condition for the left-outgoing propagation of the scattered wave can be can be written as

$$\phi_{\text{sc}}(\boldsymbol{x}) = \sum_{m=1}^{M} \mathcal{F}_m^-(\boldsymbol{x}) \phi_{m\,\text{sc}} \tag{30}$$

Therefore, substitution of $\phi_{\text{sc}} = \phi - \phi_{\text{inc}}$ yields the discretized nonreflecting inflow condition

$$\sum_{m=1}^{M^i} a_m^i \phi_m^i = b^i$$

with

$$a_m^i = \begin{cases} 1 & \text{if} \quad \boldsymbol{x}_m^i \equiv \boldsymbol{x}^i \\ -\mathcal{F}_m^{-i} & \text{otherwise} \end{cases}, \qquad b^i = \phi_{\text{inc}}^i - \sum_{m=1}^{M^i} \mathcal{F}_m^{-i} \phi_{m\,\text{inc}}^i \tag{31}$$

Method Consistency

In this section we assess the consistency of the GFD approach by computing the transmission of the right-going cut-on mode ($q = 5$, $\sigma = 2$) through an annular duct of inner radius $r_1 = 0.5$, outer radius $r_2 = 1$, and axial length $L_z = 1.15$. Computations are performed by increasing the acoustic wave number k and without changing the computational mesh. Three configurations are considered: 1) a hard-wall duct crossed by $M_\infty = 0.3$ flow, 2) a soft-wall duct without flow, and 3) a soft-wall duct with $M_\infty = 0.3$ flow. For the soft-wall configurations, only the external surface is treated with an impedance wall $\mathcal{Z} = \rho_\infty c_\infty (2 + i)$, whereas the inner surface is acoustically rigid. The computational mesh consists of $\mathcal{N}_z = 15$, $\mathcal{N}_\theta = 70$, and $\mathcal{N}_r = 15$ points in the axial, circumferential, and radial directions, respectively. A radially nonuniform mesh spacing is used; that is,

$$r = \frac{r_1 + r_2}{2} + \frac{r_1 - r_2}{2} \cos\left(\frac{i-1}{\mathcal{N}_r - 1} \pi \right), \qquad i = 1, \mathcal{N}_r \tag{32}$$

The numerical solutions are checked against the analytical ones (denoted as ϕ_a) by computing the amplitude- and phase-relative L_2 errors, defined as

$$\text{Err}_A = \sqrt{\frac{\sum_{i=1}^{\mathcal{N}} \left(|\phi^i| - \left|\phi_a^i\right| \right)^2}{\sum_{i=1}^{\mathcal{N}} \left|\phi_a^i\right|^2}}, \qquad \text{Err}_P = \frac{\sqrt{\sum_{i=1}^{\mathcal{N}} \min\{\varphi_1, \varphi_2\}}}{2\pi\sqrt{\mathcal{N}}} \tag{33}$$

where $\mathcal{N}$ is the number of grid points and

$$\varphi_1 = \left[\arg(\phi^i) - \arg\left(\phi_a^i\right) \right]^2, \qquad \varphi_2 = \left[2\pi - \left| \arg(\phi^i) - \arg\left(\phi_a^i\right) \right| \right]^2 \tag{34}$$

The influence of the computational mesh on the accuracy of the GFD scheme is illustrated by considering the number of grid points per acoustic wavelength in the axial, circumferential, and radial directions; that is,

$$N_z^\lambda = 2\pi / k\Delta z, \qquad N_\theta^\lambda = 2\pi / k r_2 \Delta\theta, \qquad N_r^\lambda = 2\pi / k\Delta r \tag{35}$$

where

$$\Delta z = L_z / (\mathcal{N}_z - 1), \qquad \Delta\theta = 2\pi / \mathcal{N}_\theta$$
$$\Delta r = (r_2 - r_1) / (\mathcal{N}_r - 1) \tag{36}$$

The stencil topologies used for these computations are shown in Fig. 1. For the nodes in the inner domain the 27-node stencil (Fig. 1a) is used. For the nodes on the boundaries both the 18-node (Fig. 1b) and the 27-node stencils (Fig. 1c) are used. The latter enables the increase of the order of the discretization scheme.

Tables 1–4 show results obtained for the three test cases. The corresponding errors are plotted against the axial grid parameter N_z^λ in Fig. 2.

The error curves in Fig. 2 show that a good level of accuracy is obtained with three points per acoustic wavelength for configurations

Table 1 Prediction of the hard-wall duct mode ($q = 5$, $\sigma = 2$, $M_\infty = 0.3$); the 18-node stencil (case 2) is used on the boundaries

k	N_z^λ	N_θ^λ	N_r^λ	Err_A	Err_P
15	5.10	4.67	11.7	$1.61E-3$	$4.86E-4$
19	4.02	3.68	9.26	$5.07E-3$	$8.22E-4$
23	3.32	3.04	7.65	$1.48E-2$	$4.18E-3$
27	2.83	2.59	6.51	$3.44E-2$	$4.66E-3$

Table 2 Prediction of the soft-wall duct mode ($q = 5$, $\sigma = 2$, $M_\infty = 0$); the 18-node stencil (case 2) is used on the boundaries

k	N_z^λ	N_θ^λ	N_r^λ	Err_A	Err_P
15	5.10	4.67	11.7	$6.17E-4$	$9.39E-5$
19	4.02	3.68	9.26	$2.22E-3$	$4.12E-4$
23	3.32	3.04	7.65	$5.69E-3$	$1.07E-3$
27	2.83	2.59	6.51	$1.06E-2$	$1.87E-3$

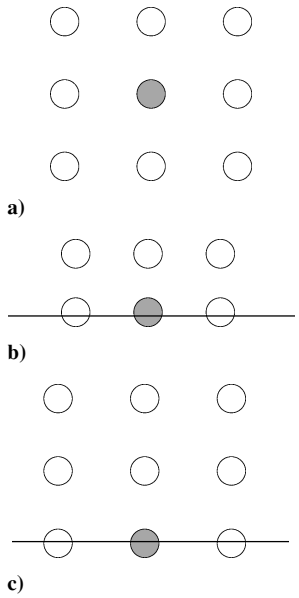

Fig. 1 Two-dimensional representation of the computational stencil for a) the inner nodes and b, c) the boundary nodes.

Table 3 Prediction of the soft-wall duct mode ($q = 5$, $\sigma = 2$, $M_\infty = 0.3$); the 18-node stencil (case 2) is used on the boundaries

k	N_z^λ	N_θ^λ	N_r^λ	Err_A	Err_P
15	5.10	4.67	11.7	$1.18E-2$	$2.45E-3$
19	4.02	3.68	9.26	$2.08E-3$	$1.59E-3$
23	3.32	3.04	7.65	$3.21E-2$	$7.14E-3$
27	2.83	2.59	6.51	$1.01E-1$	$1.72E-2$

Table 4 Prediction of the soft-wall duct mode ($q = 5$, $\sigma = 2$, $M_\infty = 0.3$); the 27-node stencil (case 3) is used on the boundaries

k	N_z^λ	N_θ^λ	N_r^λ	Err_A	Err_P
15	5.10	4.67	11.7	$1.59E-3$	$3.21E-4$
19	4.02	3.68	9.26	$7.88E-3$	$1.07E-3$
23	3.32	3.04	7.65	$1.10E-2$	$2.57E-3$
27	2.83	2.59	6.51	$2.68E-2$	$6.91E-3$

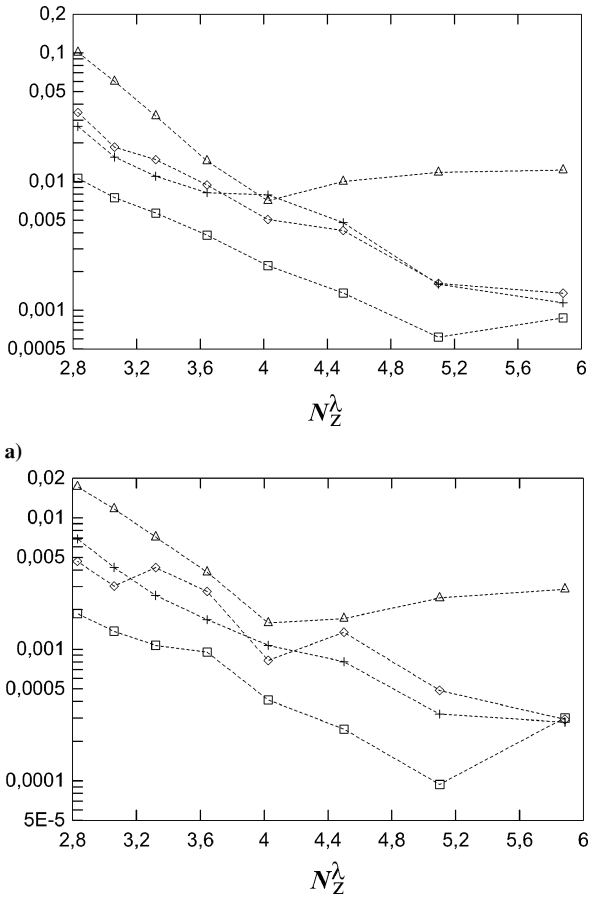

Fig. 2 Prediction of the hard- and soft-wall duct mode ($q = 5$, $\sigma = 2$). Relative L_2 error vs the axial grid parameter N_z^λ; a) amplitude error and b) phase error: ◇, hard-wall with flow; □, soft-wall without flow; △, soft-wall with flow; +, soft-wall with flow; and 27-node stencil used on the boundaries.

1 and 2. Higher errors are produced for configuration 3 unless a 27-node stencil is used on the boundaries. Indeed, impedance condition (10) involves second-order derivatives of ϕ and, thus, requires a greater number of stencil nodes to be properly discretized.

As further proof of the robustness of the GFD approach, the higher duct mode ($q = 10$, $\sigma = 3$) is computed on the same grid. The wave number is $k = 25$, the Mach number is $M_\infty = 0.3$, and the walls are rigid. The discretization factors are $N_z^\lambda = 3$, $N_\theta^\lambda = 3.06$, and $N_r^\lambda = 2.80$. Plots of the acoustic field and the local relative amplitude error are shown in Fig. 3. The amplitude- and phase-relative L_2 errors are $\mathrm{Err}_A = 2.79 \times 10^{-2}$ and $\mathrm{Err}_P = 1.86 \times 10^{-2}$, respectively.

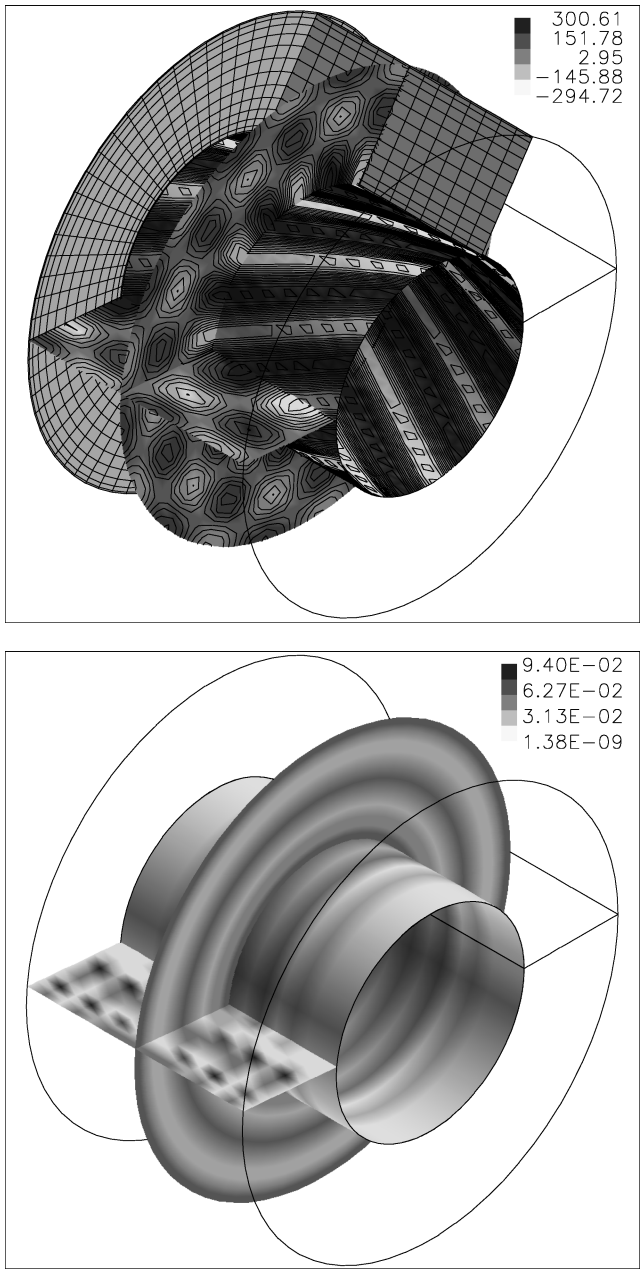

Fig. 3 Real part of the numerical potential field (top) and local amplitude error (bottom); $k = 25$, $M_\infty = 0.3$, $q = 10$, and $\sigma = 3$. Dirichlet conditions are imposed on the inlet/outlet terminations.

Nonconstant Duct Results

In this section, preliminary results for a more relevant application are presented. The GFD technique is used to compute the transmission of the right-going acoustic mode ($q = 5$, $\sigma = 2$) of wave number $k = 10$ through an annular duct of diverging cross section with/without flow and with/without acoustic treatment on the external wall. The axial duct length is $L_z = 6$, the inner radius is $r_1 = 0.5$, and the outer radius varies from $r_l = 1$ to $r_r = 1.25$ for $L_z/3 \le z \le 2L_z/3$ with the law

$$r_2(z) = (r_l + r_r)/2 + (r_l - r_r/2)\cos[(z - L_z/3)3\pi/L_z] \quad (37)$$

The computational mesh consists of $\mathcal{N}_z = 120$, $\mathcal{N}_\theta = 70$, and $\mathcal{N}_r = 15$ points in the axial, circumferential, and radial directions, respectively. Radial grid-spacing law (32) is used.

The numerical solutions are checked against the analytical ones and are obtained by using Rienstra's multiscale approach reported in Appendix C. As in Ref. 6, the numerical predictions are carried out by using the approximated mean velocity field obtained by Rienstra.[5]

a) Top: $|\phi|$, bottom: $|\phi_a|$

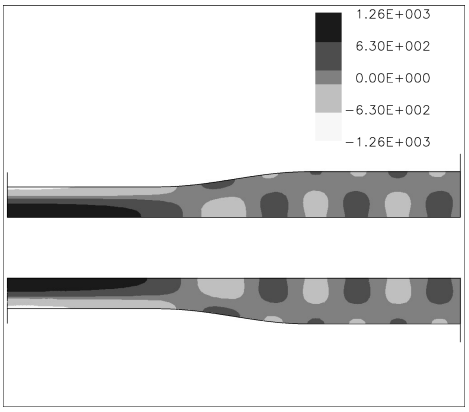

c) Top: $Re|\phi|$, bottom: $Re(\phi_a)$

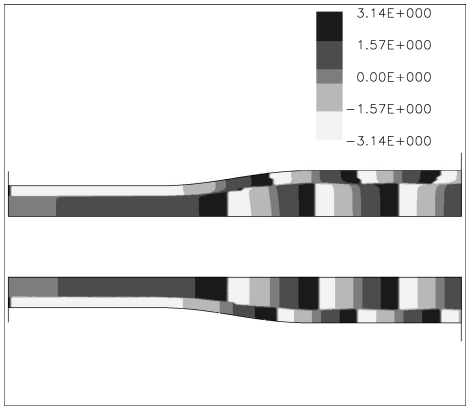

b) Top: φ, bottom: φ_a

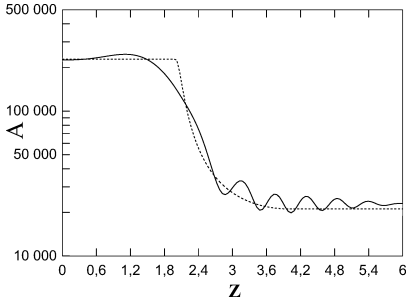

d) $A = \int_{r_1}^{r_2} |\phi(z)|^2 r\, dr$: ——, ϕ; - - - -, ϕ_a

Fig. 4 Case 1: comparison of numerical (ϕ) and analytical (ϕ_a) solutions; φ denotes the phase of ϕ.

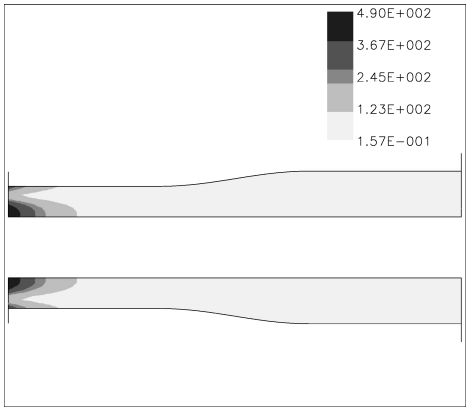

a) Top: $|\phi|$, bottom: $|\phi_a|$

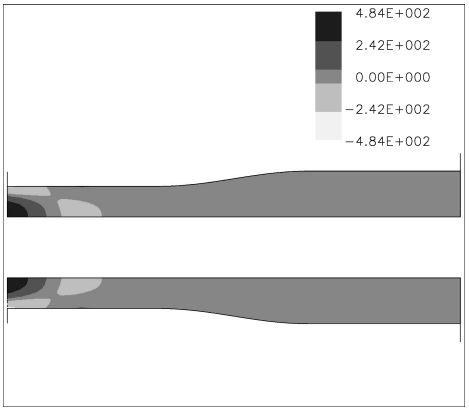

c) Top: $Re|\phi|$, bottom: $Re(\phi_a)$

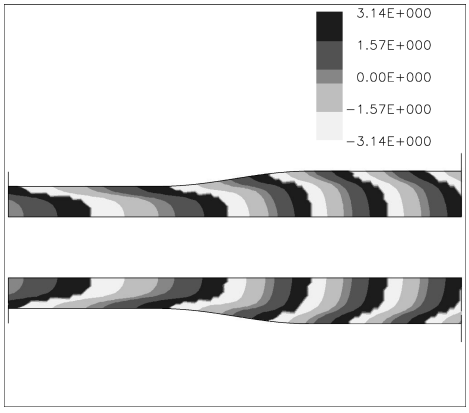

b) Top: φ, bottom: φ_a

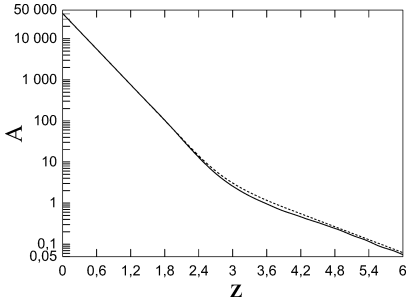

d) $A = \int_{r_1}^{r_2} |\phi(z)|^2 r\, dr$: ——, ϕ; - - - -, ϕ_a

Fig. 5 Case 2: comparison of numerical (ϕ) and analytical (ϕ_a) solutions; φ denotes the phase of ϕ.

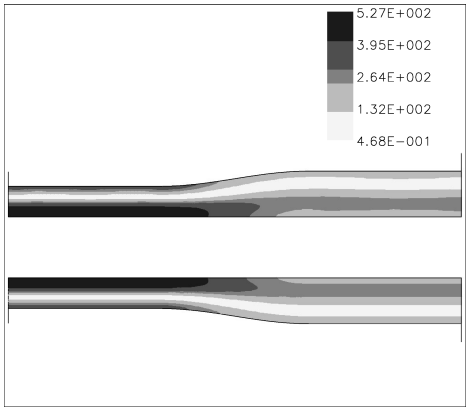

a) Top: $|\phi|$, bottom: $|\phi_a|$

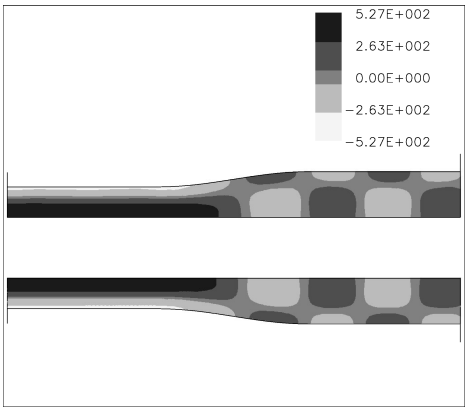

c) Top: $Re|\phi|$, bottom: $Re(\phi_a)$

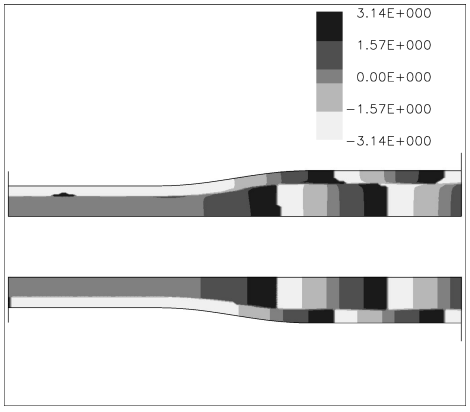

b) Top: φ, bottom: φ_a

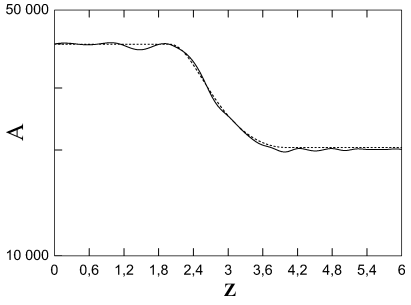

d) $A = \int_{r_1}^{r_2} |\phi(z)|^2 r\, dr$: ——, ϕ; - - - -, ϕ_a

Fig. 6 Case 3: comparison of numerical (ϕ) and analytical (ϕ_a) solutions; φ denotes the phase of ϕ.

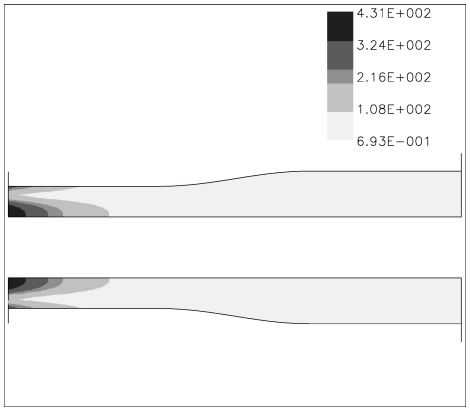

a) Top: $|\phi|$, bottom: $|\phi_a|$

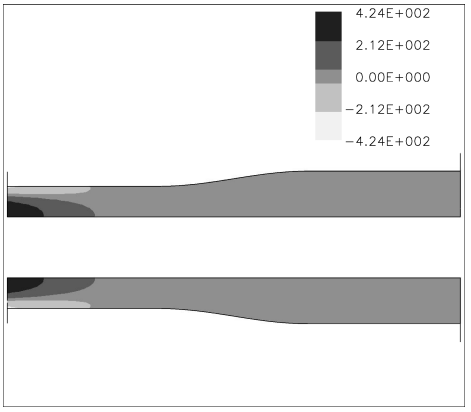

c) Top: $Re|\phi|$, bottom: $Re(\phi_a)$

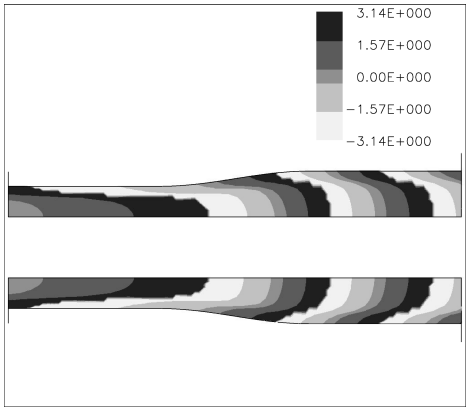

b) Top: φ, bottom: φ_a

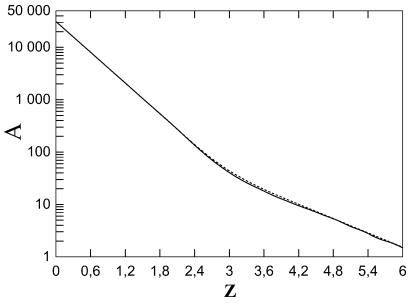

d) $A = \int_{r_1}^{r_2} |\phi(z)|^2 r\, dr$: ——, ϕ; - - - -, ϕ_a

Fig. 7 Case 4: comparison of numerical (ϕ) and analytical (ϕ_a) solutions; φ denotes the phase of ϕ.

Four cases have been considered: 1) hard-wall duct without flow, 2) soft-wall duct without flow, 3) hard-wall duct with flow, and 4) soft-wall duct with flow. For soft-wall configurations, the wall impedance on the outer surface is $\mathcal{Z} = \rho_\infty c_\infty (2 + i)$. For configurations with flow, the Mach number in the left (nondiverging) duct portion is $M_\infty = 0.3$. Computations are performed by using the 18-node stencil (Fig. 1b) for the inlet/outlet sections, and the 27-node stencil (Fig. 1c) for the inner and outer duct walls.

In Fig. 4 results for case 1 are illustrated. The compatibility of the boundary conditions with the duct modal behavior ensures a good level of accuracy. The amplitude modulation of the numerical solution (Fig. 4d) is due to a wave diffraction from the diverging section of the duct.

Results for case 2 are illustrated in Fig. 5. The agreement between numerical and analytical solution is quite good. The wave scattering effects previously observed are now controlled by the wall impedance. Therefore, no amplitude modulation occurs in the computed acoustic field. Primary results for this configuration were presented in Ref. 14. It was shown that, when hard-wall modes are employed to discretize the inlet/outlet conditions for a soft-wall duct, the numerical solution is contaminated by spurious oscillations.

Results for case 3 are illustrated in Fig. 6. The numerical and analytical solutions compare favorably. The slight amplitude modulation of the numerical solution is due to convective and geometrical scattering effects in the diverging section of the duct.

Finally, results for case 4 are shown in Fig. 7. Again, the numerical and analytical results are in quite good agreement.

Conclusions

The GFD technique was used to predict the sound transmission in ducted potential flows. A consistency study was performed by computing the propagation in a constant annular duct with and without acoustic treatment on the walls. A high level of accuracy was obtained with only three grid points per acoustic wavelength. A particular point was the advantage of using an extended computational stencil to discretize the Myers boundary condition.

A first attempt to use the GFD approach for relevant duct configurations was made by computing the propagation in a diverging duct with/without flow and with/without acoustic treatment on the walls. For the soft-wall configurations, the numerical solutions compared quite favorably with the multiscale solutions. For the hard-wall configurations, a slight axial amplitude modulation occurred in the numerical solution. This was due to wave scattering effects in the diverging section of the duct.

The next step involves applying the GFD method to realistic turbofan inlet configurations. Furthermore, in view of exhaust noise predictions, preliminary tests of duct propagation in the presence of support struts are going to be carried out.

Appendix A: Properties of the GFD Method

A first interesting aspect of the GFD approach is that, for each computational stencil, both the number of nodes and their position with respect to the collocation node i are arbitrary. Hence, a GFD code can be indifferently used with regular, irregular, structured, and unstructured meshes. The arbitrariness of the stencil definition also permits control of the order of the formulation. In the present implementation the stencil includes nodes directly connected with the node i, but a higher order formulation can be obtained by considering a second layer of nodes.

A second interesting aspect of the GFD approach lies in the peculiarity of the shape functions, which are designed specifically for the problem to be addressed. Hence, two computational stencils that are geometrically identical can have different discretization coefficients, depending on the wave number and the local flow. In comparing with the classic finite element (FE) or finite difference (FD) methods, the high accuracy and resolution of the present GFD scheme is a consequence of the narrower space in which the solutions are sought. In FE methods, the shape functions are such that, with a sufficiently refined discretization, they can model a completely generic function. In the GFD method, on the contrary, the shape functions can describe only the specific set of functions that locally satisfy the wave equation for a given wave number. Therefore, even if the discretization were greatly refined, it would be impossible to reconstruct a generic field (e.g., a constant one) that is not a solution of the wave equation for the considered wave number. In FD methods, the sum of the discretization coefficients of a generic derivative is identically zero, allowing the reconstruction of a constant solution. This property is not respected by the GFD scheme, because a constant field is not a solution of the wave equation for a nonzero wave number. Interestingly, for a vanishing wave number, the GFD method provides discretization coefficients that are identical to those of an FD method.

Appendix B: Hypersphere

In the GFD scheme described in Ref. 8, the fictitious sources are distributed over the four-dimensional hypersphere:

$$x_n = r\cos(\psi_n)\cos(\beta_n)\cos(\alpha_n)$$

$$y_n = r\cos(\psi_n)\cos(\beta_n)\sin(\alpha_n)$$

$$z_n = r\cos(\psi_n)\sin(\beta_n), \qquad w_n = r\sin(\psi_n)$$

where n is the cumulative index over the polar indices (i, j, k) providing

$$\psi_n = 2\pi k/N_3, \qquad k = 1, N_3$$

$$\beta_n = -\pi/2 + \pi j/(N_2 + 1), \qquad j = 1, N_2$$

$$\alpha_n = 2\pi i/N_2 + 2\pi j/N_1 N_2, \qquad i = 1, N_1$$

The poles $[0, 0, \mp r\cos(\psi_n), r\sin(\psi_n)]$ are also included.

In the present paper, the governing wave equation is discretized by distributing $N = 217$ sources over two spheres: a hypershere of radius $r = 200\lambda$ and parameters $N_1 = 3$, $N_2 = 3$, and $N_3 = 3$, and a sphere of radius $r = 20\lambda$ and parameters $N_1 = 14$, $N_2 = 13$, and $N_3 = 1$. Boundary conditions are discretized by distributing $N = 184$ sources over a sphere of radius $r = 20\lambda$ and parameters $N_1 = 14$, $N_2 = 13$, and $N_3 = 1$. The quantity λ denotes the acoustic wavelength.

Appendix C: Soft-Wall Slowly Varying Duct

Consider an annular duct with nonconstant properties: cross section, flow, and wall impedance. A multiscale solution has been obtained by Rienstra[5] by supposing slowly varying properties. It has been used in this paper to validate the numerical solutions.

The multiscale method is based on the hypothesis that the length scale of a geometrical (flow) variation is much smaller than the duct diameter. The slow variable $Z = \epsilon z$ can therefore be used as an explicit variable, where ϵ denotes the ratio between the variation length scale and the duct diameter.

A ducted axisymmetrical mean flow can be written as

$$\boldsymbol{M} = M_z(Z, r; \epsilon)\boldsymbol{e}_z + M_r(Z, r; \epsilon)\boldsymbol{e}_r \tag{C1}$$

where the axial dimensionless velocity can be related to a given (dimensionless) cross-sectional mass flux F by writing

$$M_z(z) = \frac{\rho_\infty r_\infty^2 F}{\Theta(z)\left[r_2(z)^2 - r_1(z)^2\right]} \tag{C2}$$

In a slowly varying duct the mean flow is nearly uniform: its axial component depends only on Z, and small axial mass variations can only be balanced by a small radial flow component. We can therefore write

$$M_z(Z, r; \epsilon) = M_0(Z) + O(\epsilon^2) \tag{C3}$$

$$M_r(Z, r; \epsilon) = \epsilon M_1(Z, r) + O(\epsilon^3) \tag{C4}$$

$$P(Z, r; \epsilon) = P_0(Z) + O(\epsilon^2) \tag{C5}$$

$$\Theta(Z, r; \epsilon) = \Theta_0(Z) + O(\epsilon^2) \tag{C6}$$

where

$$P_0(Z) = p_\infty\left\{1 - [(\gamma-1)/2]\left[M_0(Z)^2 - M_\infty^2\right]\right\}^{\gamma/(\gamma-1)} \quad \text{(C7)}$$

$$\Theta_0(Z) = \rho_\infty\left\{1 - [(\gamma-1)/2]\left[M_0(Z)^2 - M_\infty^2\right]\right\}^{1/(\gamma-1)} \quad \text{(C8)}$$

The axial velocity is given by

$$M_0(Z) = \frac{\rho_\infty r_\infty^2 F}{\Theta_0(Z)\left[r_2(Z)^2 - r_1(Z)^2\right]} \quad \text{(C9)}$$

where the mean density $\Theta_0(z)$ is to be determined numerically, for a given value of M_∞, by using Eq. (C8).

Making use of the so-called WKB (Wentzel, Kramers, and Brillouin) assumption, the acoustic potential can be described as a superposition of modelike solutions of the form

$$\phi_{q\sigma}(z, r, \theta; \epsilon) = \Phi(Z, r; \epsilon)\exp\left[iq\theta + i\int^z \mu(\xi)\,\mathrm{d}\xi\right] \quad \text{(C10)}$$

where $\mu(Z)$ is the axial wave number. By expanding $\Phi = \Phi_0(Z, r) + \epsilon\Phi_1(Z, r) + \cdots$ and $\mu = \mu_0 + O(\epsilon^2)$, and substituting in the governing equations and Myers's boundary condition of wall impedance $\mathcal{Z}$, Rienstra[5] obtained a Bessel-type equation in r for Φ_0, which allows us to write the slowly varying mode as

$$\Phi_0(Z, r) = N(Z)J_q[\alpha(Z)r] + M(Z)Y_q[\alpha(Z)r] \quad \text{(C11)}$$

The radial eigenvalue α and the ratio M/N are determined by boundary conditions. These yield

$$\frac{\alpha r_2 J_q'(\alpha r_2) - \zeta_2 J_q(\alpha r_2)}{\alpha r_2 Y_q'(\alpha r_2) - \zeta_2 Y_q(\alpha r_2)} = \frac{\alpha r_1 J_q'(\alpha r_1) + \zeta_1 J_q(\alpha r_1)}{\alpha r_1 Y_q'(\alpha r_1) + \zeta_1 Y_q(\alpha r_1)} = -\frac{M(Z)}{N(Z)} \quad \text{(C12)}$$

where

$$\zeta_i = \frac{\mathrm{i}\Omega^2\Theta_0 r_i}{\omega\mathcal{Z}_i}, \qquad i = 1, 2 \quad \text{(C13)}$$

$$\Omega = c_\infty(k - \mu_0 M_0) \quad \text{(C14)}$$

$$\mu_0 = -\frac{M_0 k_0}{\beta_0^2} \pm \frac{1}{\beta_0^2}\sqrt{k_0^2 - \beta_0^2\alpha^2} \quad \text{(C15)}$$

$$k_0 = \frac{\omega}{C_0} \quad \text{(C16)}$$

$$\beta_0^2 = 1 - \frac{c_\infty^2 M_0^2}{C_0^2} \quad \text{(C17)}$$

Finally, the amplitude $N(Z)$ is such that

$$\left(\frac{\pi/2}{N}\right)^2 E_0 = \left[\frac{\Theta_0 k_0 \Lambda r_2^2}{2}\left(1 - \frac{j^2 - \zeta_2^2}{\alpha^2 r_2^2}\right) + \frac{\Theta_0 M_0 c_\infty}{\Omega}\zeta_2\right]\Bigg/ [\alpha r_2 Y_q'(\alpha r_2) - \zeta_2 Y_q(\alpha r_2)]^2$$

$$-\left[\frac{\Theta_0 k_0 \Lambda r_1^2}{2}\left(1 - \frac{j^2 - \zeta_1^2}{\alpha^2 r_1^2}\right) - \frac{\Theta_0 M_0 c_\infty}{\Omega}\zeta_1\right]\Bigg/ [\alpha r_1 Y_q'(\alpha r_1) + \zeta_1 Y_q(\alpha r_1)]^2 \quad \text{(C18)}$$

where $\Lambda = \pm\sqrt{(1 - \beta_0^2\alpha^2/k_0^2)}$ and E_0 is an arbitrary integration constant having the dimensions of energy. The square root to be chosen is such that the continuity of N along Z is ensured. The preceding analytical expression is equally valid for hollow and annular ducts and constitutes the main result of Rienstra's formulation.

Acknowledgment

The authors are grateful to Paolo di Francescantonio for his valuable comments.

References

[1]Tester, B. J., "Some Aspects of 'Sound' Attenuation in Lined Ducts Containing Inviscid Mean Flows with Boundary Layers," *Journal of Sound and Vibration*, Vol. 28, 1973, pp. 217–245.

[2]Myers, M. K., "On the Acoustic Boundary Condition in the Presence of Flow," *Journal of Sound and Vibration*, Vol. 71, No. 3, 1980, pp. 429–434.

[3]Golubev, V. V., and Atassi, H. M., "Sound Propagation in an Annular Duct with Mean Potential Swirling Flow," *Journal of Sound and Vibration*, Vol. 198, No. 5, 1996, pp. 601–616.

[4]Golubev, V. V., and Atassi, H. M., "Acoustic-Vorticity Waves in Swirling Flows," *Journal of Sound and Vibration*, Vol. 209, No. 2, 1998, pp. 203–222.

[5]Rienstra, S. W., "Sound Transmission in Slowly Varying Circular and Annular Lined Ducts with Flow," *Journal of Fluid Mechanics*, Vol. 380, 1999, pp. 279–296.

[6]Rienstra, S. W., and Eversman, W., "A Numerical Comparison Between the Multiple-Scales and Finite-Element Solution for Sound Propagation in Lined Flow Ducts," *Journal of Fluid Mechanics*, Vol. 437, 2001, pp. 367–384.

[7]Cooper, A. J., and Peake, N., "Propagation of Unsteady Disturbances in a Slowly Varying Duct with Mean Swirling Flow," *Journal of Fluid Mechanics*, Vol. 445, 2001, pp. 207–234.

[8]Di Francescantonio, P., and Casalino, D., "Green's Function Discretization Scheme for Sound Propagation in Nonuniform Flows," *AIAA Journal*, Vol. 37, No. 10, 1999, pp. 1161–1172.

[9]Casalino, D., "Un Metodo Numerico per lo Studio dello Scattering e della Propagazione del Suono in Mezzi non Omogenei," M.S. Thesis, Dipartimento di Ingegneria Aeronautica e Spaziale, Politecnico di Torino, Turin, Italy, 1997.

[10]Astley, R. J., and Bain, J. G., "A Three-Dimensional Boundary Element Scheme for Acoustic Radiation in Low Mach Number Flows," *Journal of Sound and Vibration*, Vol. 109, No. 3, 1986, pp. 445–465.

[11]Caruthers, J. E., French, J. C., and Raviprakash, G. K., "Green's Function Discretization for Numerical Solution of the Helmholtz Equation," *Journal of Sound and Vibration*, Vol. 187, No. 4, 1995, pp. 553–568.

[12]Caruthers, J. E., Engels, R. C., and Raviprakash, G. K., "A Wake Expansion Computational Method for Discrete Frequency Acoustic Within Inhomogeneous Flows," AIAA Paper 96-1684, May 1996.

[13]Caruthers, J. E., French, J. C., and Raviprakash, G. K., "Recent Developments Concerning a New Discretization Method for the Helmholtz Equation," AIAA Paper 95-117, May 1995.

[14]Casalino, D., Roger, M., and Jacob, M., "Prediction of Sound Propagation in Ducted Potential Flows Using Green's Function Discretization," AIAA Paper 2003-3246, May 2003.

M. Ahmadian
Associate Editor